Computational Mechanics manuscript No.
(will be inserted by the editor)

R. Laniel · P. Alart · S. Pagano

Discrete element investigations of wire-reinforced geomaterial in a three-dimensional modeling

Received: date / Accepted: date

Abstract The aim of the study is to build discrete numerical models of a wire-reinforcement for geomaterials to perform multi-scale investigations. Non Smooth Contact Dynamics is used to carry out large or small strain mechanical tests on a granular sample. Different numerical experiments distinguish the main reinforcement micro-mechanisms and their consequences for macroscopic behavior.

Keywords geomaterial · discrete modeling · wire reinforcement · unilateral law

1 Investigation context

The discrete element investigations presented in this paper concern a reinforced granular material. The scope of the study is an attempt to homogenize this material and will be introduced in this section.

1.1 A soil reinforcement process: the *TexSol*™

Civil engineers are often expected to build larger and larger constructions; the ground needs assistance in supporting such works. Various solutions can be used to reinforce soil, columns, micro-piles, geomembranes, geogrids and geotextiles. This paper focuses on a particular process, belonging to the last reinforcement category: *TexSol*™. It is a soil reinforcement process created in 1984 by Leflaive, Khay and Blivet from the LCPC (Laboratoire Central des Ponts et Chaussées) [9; 12]. It is original in that it combines the soil (sand) with wire. A machine, called a "texsoleuse", does this by depositing sand and feeding in the wire at the same time. The latter is randomly distributed on the free surface and is simultaneously covered with sand to create a *TexSol*™ layer. Although the wire volume is negligible compared to that of the sand, the wire becomes a strong reinforcement when it tangles up inside the sand. This type of material is adapted for embankments requiring a strong slope or works which may be subjected to dilatation strain (protection dome of a gas reserve for example). Indeed, the wire works in tensile directions and the wire network maintains the structure (when wire density is high enough); *TexSol*™ can be regarded as a composite material. But the reinforcement micromecanisms remain relatively obscure. The macroscopic maintenance of the structure can be roughly explained by phenomena like tangles or remote forces even if these are difficult to highlight and to quantify.

R. Laniel
LMGC, UMR CNRS 5508, Université Montpellier II, CC 048
Place Eugène Bataillon, 34095 Montpellier cedex 5, France
Tel.: +334-67-144537
E-mail: laniel@lmgc.univ-montp2.fr

1.2 Interest of continuous modeling

On the macroscopic scale, it is useful for engineers to have continuous models of their materials (to insert in a finite element code) to predict structural behavior. Two kinds of continuous modeling are found in the literature for geomaterials reinforced by wire. The first model suggested by Fremond in [7] is non local and includes remote interactions (corresponding to the wire effects). This model also takes wire breaking potential into account. A second, local model is proposed by Villard in [19] coupling a standard model of sand with an equivalent unilateral elastic stiffness for the wire network. The unilateral characteristic of this feature means that stiffness is only activated in tensile directions. A local model was created from the previous one, in a coherent thermodynamic framework [13]. We give in [10] two thermodynamic potentials. The first is *TexSol*™ free energy,

$$\psi_t(\boldsymbol{\varepsilon}, \boldsymbol{\varepsilon}^p, \boldsymbol{\alpha}, p) = \mathscr{E}_s(\boldsymbol{\varepsilon}, \boldsymbol{\varepsilon}^p) + \mathscr{E}_w^+(\boldsymbol{\varepsilon}) + \mathscr{H}_s(\boldsymbol{\alpha}, p) \ . \qquad (1)$$

The state and internal variables are respectively, total strain, plastic strain, kinematic and isotropic hardening variables; this potential is defined as the sum of sand elastic energy, the unilateral elastic energy of the wire

network and the sand hardening energy. The second potential is the Legendre – Fenchel transform of *TexSol*$^{\mathrm{TM}}$ dissipation potential,

$$\varphi_t^*(\boldsymbol{\sigma}^{\mathrm{ir}}, \boldsymbol{A}, \boldsymbol{\chi}, R) = \mathrm{I}_{\{\mathbf{0}\}}(\boldsymbol{\sigma}^{\mathrm{ir}}) + \mathrm{I}_{\Omega(\boldsymbol{\chi},R)}(\boldsymbol{A}) \ . \tag{2}$$

The state variable $\boldsymbol{\sigma}^{\mathrm{ir}}$ is the irreversible strain and the internal variables are the conjugate of $\boldsymbol{\varepsilon}^p$, $\boldsymbol{\alpha}$ and p; I_D is the indicator function of a set D and Ω is the Drucker – Prager elastic domain in the principal-stresses space. State laws and complementary laws were derived from these potentials. The model previously described is valid within the small strain framework and must validate the assumptions of stress additivity $\boldsymbol{\sigma}_t = \boldsymbol{\sigma}_s + \boldsymbol{\sigma}_w$ and strain rate equalities $\dot{\boldsymbol{\varepsilon}}_t = \dot{\boldsymbol{\varepsilon}}_s = \dot{\boldsymbol{\varepsilon}}_w$ between the *TexSol*$^{\mathrm{TM}}$, the sand and the wire respectively described by subscripts t, s and w. The study of a numerical discrete *TexSol*$^{\mathrm{TM}}$ model enables us to compare the macroscopic behavior of a heterogeneous sample with an equivalent continuous model.

1.3 An identification approach based on discrete numerical experiments

It is classical to identify the material parameters (stiffness, hardening et cætera) in a continuous model of a complex structure, by carrying out a backward analysis. Moreover, Finite Element Method Updating (FEMU) is an iterative method varying the material parameters set Θ to minimize a cost function $J(\Theta)$ [1] (cf. table 1). This function represents the error between the measured value fields and those computed by the finite element method. Experimental tests are generally used to update the set

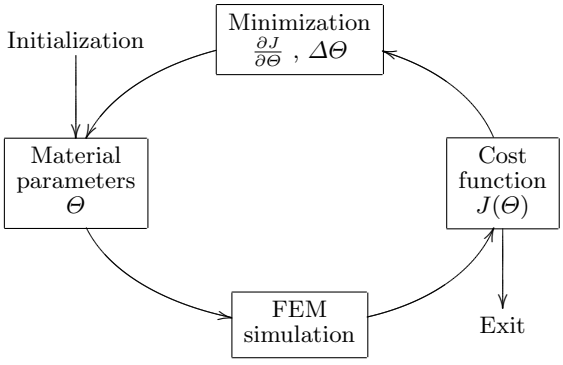

Table 1 FEMU algorithm.

parameters but the measurable fields are limited (surface strain, partial displacement field, total force on boundary conditions). In our approach, the measure fields are replaced by discrete numerical experiments. Thus, all the particle displacements and contact forces can be extracted from the sample. By locally averaging the previous fields, the equivalent stress and strain tensors of the granular material are built up [2; 5; 15]. These provide more accurate information than the experimental method with a more relevant cost function.

2 Discrete element modeling

As *TexSol*$^{\mathrm{TM}}$ is a reinforced granular material, the sand matrix can be perfectly integrated in discrete modeling. However, the continuous nature of the wire requires a specific modeling effort.

2.1 Non Smooth Contact Dynamics (NSCD) approach

The NSCD is a discrete element method used in the *LMGC90* code which simulates multibody vs. multicontact problems, privileging velocity fields [8]. For a rigid body collection, let us consider q and R the Lagrange coordinate vector and the contact reactions, torques vector (reactions imposed on a candidate particle by the neighbour ones) respectively. The dynamic equations are expressed as follows

$$M\ddot{q}(t) = F_{\mathrm{ext}}(t) + R \ , \tag{3}$$

where F_{ext} and M are the external forces and mass matrix respectively. The integration scheme of the NSCD is a θ-method with θ ranging between 0.5 and 1 to be unconditionally stable. The evolution law of q is written on the interval $]t_i, t_{i+1}]$ with a time step h and the velocity, free of contacts is defied as $\dot{q}_{\mathrm{free}}$,

$$\begin{array}{l} q_{i+1} = q_i + \theta\dot{q}_{i+1} + (1-\theta)\dot{q}_i \\ \dot{q}_{\mathrm{free},i+1} = \dot{q}_i + hM^{-1}(\theta F_{\mathrm{ext},i+1} + (1-\theta)F_{\mathrm{ext},i}) \ . \end{array} \tag{4}$$

For a single contact α problem, the NSCD evaluates the external forces and dynamic effects on the contactor point. To make such a transformation, H_α and H_α^T are used to move variables from the local contact frame to the global body and vice-versa. The local contact α variables u^α and r^α (respectively the relative velocity and the contact reactions in the contact local frame) are defined with $u^\alpha = H_\alpha^T\dot{q}$ and $R = H_\alpha r^\alpha$. We also introduce the average impulsion $p^\alpha = \int_{t_i}^{t_{i+1}} r^\alpha \mathrm{d}t$ and can write

$$\left\{ \begin{array}{l} u_{i+1}^\alpha - W^{\alpha\alpha}p_{i+1}^\alpha = u_{\mathrm{free},i}^\alpha + \sum_{\beta\neq\alpha} W^{\alpha\beta}p_{i+1}^\beta \\ \mathrm{Law}[u_{i+1}^\alpha, p_{i+1}^\alpha] = \mathrm{true} \ . \end{array} \right. \tag{5}$$

The smooth dynamic effects are included in the expression of the relative free velocity $u_{\mathrm{free},i}^\alpha$. The Delassus operator $W^{\alpha\beta} = H_\alpha^T M^{-1} H_\beta$ naturally appears in the dynamics reduced to contacts. In this way, for a frictionless problem with a Signorini contact condition, the system (5) reveals to be a standard Linear Complementarity Problem (LCP),

$$\left\{ \begin{array}{l} u_{i+1} - Wp_{i+1} = u_{\mathrm{free},i} \\ 0 \leq u_{i+1} \perp p_{i+1} \geq 0 \ . \end{array} \right. \tag{6}$$

For a frictional contact problem, tangential reactions and tangential velocities have to verify a similar non smooth relation. A Gauss – Seidel loop computes all contact reactions until convergence.

2.2 Discrete wire modeling

In the *NSCD*, a body is represented by its gravity center, its mass, its inertia moments and a set of contactors (*sphere*, *plan*, *polyheron*, *point* et cætera). These describe the object material border used by *LMGC90* in the contact detection process which creates contact elements between two contactors (*sphere-sphere* for example). To discretize the wire, it is broken up into a collection of equidistant material points, with the wire mass equal to the sum of all point masses. All these points must be connected by a behavior law which accounts for a small segment of wire. The wire must keep its free flexion and unilaterality properties. Consequently, a wire contact law concerns only the normal direction and there is no constraint on the tangential directions. In all cases, flexion is imposed and mesoscopic unilaterality can be seen, as, in longitudinal compression, the discrete wire (more than two points) behaves like a buckling beam. The contactors used to support these laws are *points* located at the gravity centers. Thus, four laws can be introduced (cf. Fig. 2, 3) implemented in *LMGC90*, corresponding to four different wire behaviors.

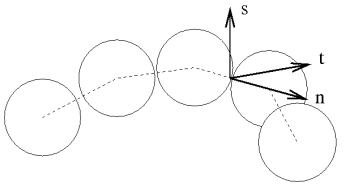

Fig. 1 Discrete wire modeled by a chain of beads with a local contact frame.

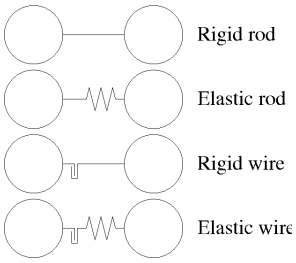

Fig. 2 Schematic representation of different wire interaction laws on the normal axis.

- ***"Rigid rod"***: this is the simplest contact law used for the wire. It couples the normal velocity of both candidate and antagonist particles

$$u_n = 0 \; ; \; p_n \in \mathbb{R} \; \Rightarrow \; g = g_{\text{ref}} \; , \tag{7}$$

where $g = g^+ = g(t_{i+1})$ is the minimum distance between two contactors (referred to as a gap) at the end of the considered time step (in opposition to $g^- = g(t_i)$, the gap at the beginning of the considered time step) and $g_{\text{ref}} = \frac{g(0)}{1+\varepsilon_0}$ is the gap with no force and no displacement on the contact element (ε_0 is the prestrain). Let us introduce two variable changes on u_n and p_n,

$$\begin{array}{l} \widetilde{u}_n = \frac{g_{\text{ref}} - g^-}{h} - u_n \\ \widetilde{p}_n = -p_n \; . \end{array} \tag{8}$$

The previous interaction law then becomes,

$$\widetilde{u}_n = 0 \; ; \; \widetilde{p}_n \in \mathbb{R} \; . \tag{9}$$

- ***"Elastic rod"***: this law adds regularisation (due to elasticity k) to the contact problem in both compression and tensile directions.

$$p_n = -h^2 k \left(u_n - \frac{g_{\text{ref}} - g^-}{h} \right) \; . \tag{10}$$

Expressed with $\widetilde{u}_n$ and $\widetilde{p}_n$ this condition becomes,

$$\widetilde{p}_n = -h^2 k \widetilde{u}_n \; . \tag{11}$$

- ***"Rigid wire"***: this is a **unilateral** law which can be described by,

$$u_n \leq \frac{g_{\text{ref}} - g^-}{h} \; , \; p_n \leq 0 \; , \; u_n p_n = 0 \; . \tag{12}$$

With variables $\widetilde{u}_n$ and $\widetilde{p}_n$ a classical LCP is obtained,

$$0 \leq \widetilde{u}_n \perp \widetilde{p}_n \geq 0 \; . \tag{13}$$

- ***"Elastic wire"***: this includes unilaterality and the wire stiffness parameter k,

$$p_n = \begin{cases} 0 & \text{if } u_n \leq \frac{g_{\text{ref}} - g^-}{h} \\ -h^2 k \left(u_n - \frac{g_{\text{ref}} - g^-}{h} \right) & \text{if } u_n \geq \frac{g_{\text{ref}} - g^-}{h} \end{cases} \; . \tag{14}$$

If we consider another variable change, $\widehat{u}_n = \frac{g_{\text{ref}} - g^-}{h} - u_n - \frac{p_n}{h^2 k}$, the previous condition can be written as a LCP (like all unilateral interaction laws),

$$0 \leq \widehat{u}_n \perp \widetilde{p}_n \geq 0 \; . \tag{15}$$

This law may be interesting to implement in *LMGC90* (cf Sect. 1.2) since the behavior of the wire network is elastic in our continuous model.

An advantage of the "Unilateral" laws is that the returned reaction on the contact element *point-point* is only tensile, better accounting for the wire behavior. To ensure the relevance of the model, a discrete wire was loaded under gravity by fixing both ends. For the "Rigid" laws, the position (x, y) of the material points obtained at the end of the test, agrees with the classic equation $y - y_0 = a \cosh\left(\frac{x - x_0}{a}\right)$, where the parameters a, x_0 and y_0 have to be identified. The "Elastic" laws also provide results very close to the previous solution if the specific masses do not involve too much strain in the wire. Another test reserved for the "Elastic" laws, consists in initializing a discrete wire under tension according to the first vibrating mode of the chord. For a sufficiently small time step, the principal frequencies between the computed solution and that found using the vibrating chord equation are close, $y(x,t) = A \sin(-\pi \frac{vt}{L})$, $v = (\frac{F}{\mu})^{1/2}$. Parameters μ, F, L and t are respectively

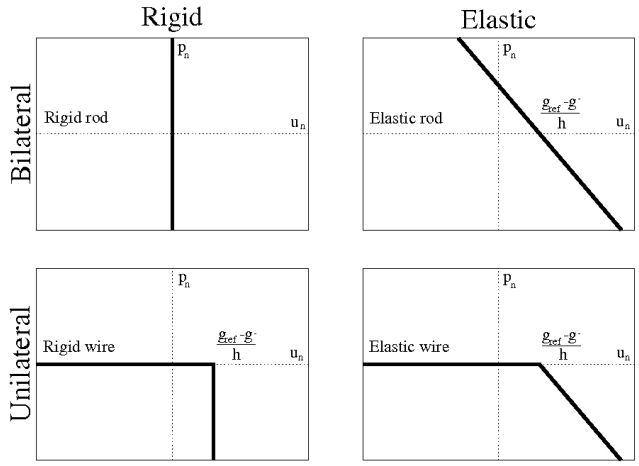

Fig. 3 Velocity graphs of the four wire interaction laws.

linear mass density, wire tension, wire length and time. Finally, to ensure the interactions between the wire and the sand, *spheres* (as contactors) are attached to all material *points*. This allows the wire to be modeled by a chain of beads (cf. Fig. 1).

2.3 Why three-dimensional modeling ?

It is easier to work with a discrete *TexSol*$^{\mathrm{TM}}$ sample in two-dimensional modeling [11; 16] (*TexSol*$^{\mathrm{TM}}{}_{\mathrm{2D}}$). This study is a first approximation providing some answers to the question: What kind of action mode does wire reinforcement have on the sand ? In the two-dimensional environment of *LMGC90*, the sand is modeled by a collection of *disks* and the wire network by a chain of beads. The *TexSol*$^{\mathrm{TM}}{}_{\mathrm{2D}}$ sample is built with a geometrical thickening preprocessor (its three-dimensional extension is explained in Sect. 2.4) which is then subjected to a biaxial test. This is equivalent to a deviatoric load, on a material under pressure, due to a force increment or velocity on the upper bound. In this example, only the "Rigid" models are used and the behavior of the "Unilateral" or "Bilateral" laws are analyzed with the force vs. crushing graphs of each material in Fig. 4. The two "Rigid" laws provide the same reinforcement up to a critical crushing level where an extra reinforcement occurs with the "Rigid Rod" law. This phenomenon is explained by the formation of a wire column involving compression and not tensile state. In this way the wire contributes to the vertical strength of the sample. This occurrence is amplified by two-dimensional modeling. Moreover, two-dimensional modeling introduces an artificial membrane effect which is not reproduced in a real three-dimensional simulation. In some regions, the sand grains are confined by a chain of bead behaving like a membrane as shown in Fig. 5. Finally, these drawbeads are required to carry out three-dimensional modeling.

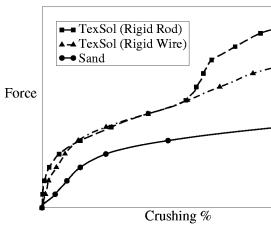

Fig. 4 Biaxial test of sand and *TexSol*$^{\mathrm{TM}}{}_{\mathrm{2D}}$ samples using unilateral and bilateral laws [16].

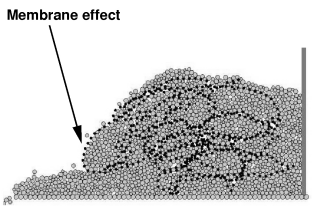

Fig. 5 Representation of the *TexSol*$^{\mathrm{TM}}{}_{\mathrm{2D}}$ reinforcement mechanism [16].

2.4 How to prepare a numerical *TexSol*$^{\mathrm{TM}}$ sample

The simulation of granular media requires starting from an initial configuration characterized not only by its geomaterial particle distribution but also by the force network obtained at the end of a numerical preparation close enough to a realistic *TexSol*$^{\mathrm{TM}}$ sample. As mentioned in Sect. 1.1, the two main features to reproduce are the entanglement of the wire through the sand and the stress network deriving from it.

The first step is to distribute the wire in a container (box, cylinder, sphere et cætera); this is built bead by bead. Let us consider a particle i of center $X_i = (x_i, y_i, z_i)$,

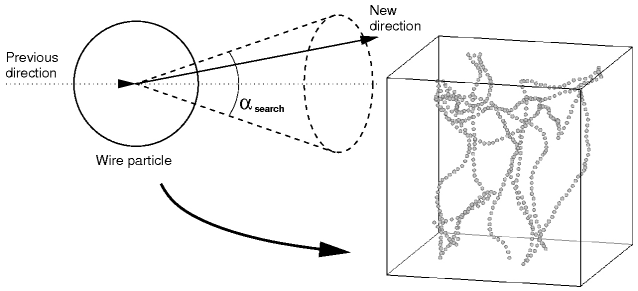

Fig. 6 Example of a wire generating process in a box.

radius r_w and a gap g_w between each wire particles. For an isotropic wire network, the reference direction is defined by,

$$\mathfrak{y}_{\mathrm{ref}} = \begin{cases} \mathfrak{y}_{\mathrm{ini}} & \text{if } i = 1 \\ \mathfrak{y}_i = (X_i - X_{i-1})^{\mathbb{1}} & \text{if } i \neq 1 \ , \end{cases} \tag{16}$$

where $\mathfrak{y}_{\mathrm{ini}}$ is an initial normalized direction and $X^{\mathbb{1}}$ is the normalized vector of X defined by $X^{\mathbb{1}} = \frac{X}{||X||}$. The following random direction $\mathfrak{y}_{i+1}$ has to belong to a cone of axis $\mathfrak{y}_{\mathrm{ref}}$ and angle α_{search} called the research angle; the position of the particle $i+1$ is $X_{i+1} = X_i + (2r_w + g_w)\mathfrak{y}_{i+1}$ (cf. Fig. 6). If after n random pullings the new particle always intersects a previous one or is always outside

the container, the following random pulling is performed using a new increased angle α_{search} taken equal to $\frac{4\pi}{3}$ (respectively "Bypassing" or "Rebound" procedure). If these procedures do not give an acceptable solution, the wire is broken and a new wire started again elsewhere. The random distribution is conditioned by associating the research cone and the recursive continuation $\mathfrak{y}_i$. For an orthotropic wire required by samples where the wire is laid out in horizontal layers, the reference direction is modified as follows,

$$\mathfrak{y}_{\text{ref}} = \begin{cases} \mathfrak{y}_{\text{ini}} & \text{if } i = 1 \\ \begin{Bmatrix} x_i - x_{i-1} \\ y_i - y_{i-1} \\ \sin(\alpha_{\text{rise}}) \end{Bmatrix}^{\mathbb{1}} & \text{if } i \neq 1 \ , \end{cases} \tag{17}$$

where α_{rise} is a small constant parameter called the rise angle. In the orthotropic case, the vertical component of X_i is computed around a constant value.

Once the wire is generated, the sand particles have to be created in the container. The two-dimensional geometrical deposit method developed by Taboada [18] has been extended to three-dimensional problems. Its principle consists in placing a new spheric particle onto the free surface of previously deposited grains, minimizing an energetic criterion (in our study, the potential energy). In the simplest case, a list of sphere triplets must be found on which to place the new particle. The final position of the sphere on the optimal triplet is established by solving a large number of 2$^{\text{nd}}$ degree equations discriminated with the previous energetic criterion. If the polydispersity of the collection of grains (ratio of the biggest sphere radius over the smallest) is wide enough, a small sphere may be placed inside the sample and not only on the free surface. Specific triplet selection procedures have been developed to get samples as dense as possible. At this stage the sample is only geometrically admissible. A deposit is then made under gravity to relax the sample and to obtain the force network. Consequently, the geometry is modified, namely wire tortuosity ξ is amplified as shown in Fig. 7. We chose to define the tortuosity coefficient by $\xi = \frac{1}{l}\int \rho^{-1}(s)ds$ with l the wire length and $\rho(s)$ the curvature radius at the curvilinear abscissa s. Moreover, the previous strategy decreases the make-ready time from 2 days to 2 hours for a 40000 particle sample compared with a classic deposit process starting from a periodic grid repartition.

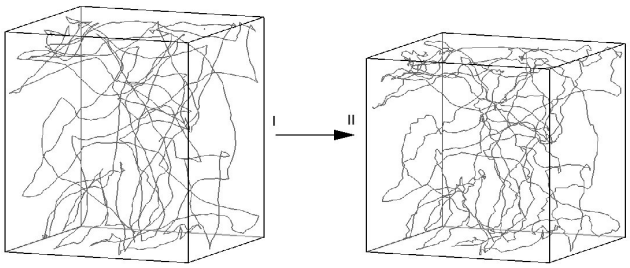

Fig. 7 Tortuosity evolution of a wire network before (I) and after (II) a deposit under gravity from $\xi_{\text{I}} = 839$ m^{-1} to $\xi_{\text{II}} = 1464$ m^{-1}.

3 Mechanical tests

Once the *TexSol*$^{\text{TM}}$ sample clearly generates as a granular media (with the preprocessor described previously), mechanical tests can be carried out. Large vs. small strain tests are distinguished to emphasize the differences in reinforcement mechanisms. First a qualitative test on a *TexSol*$^{\text{TM}}$ slope highlights the reinforcement mechanisms often associated with this special material. Second, triaxial tests on cylindrical samples are carried out and some macroscopic information such as strain or stress tensor is computed.

3.1 Qualitative test on a *TexSol*$^{\text{TM}}$ slope

This test consisted in depositing a geometrically densified sample on a rubber plan assimilated to a collection of equal radius beads in a hexagonal distribution. The initial sample represented in Fig. 8 was a cylinder-shaped ∅ 12 mm in diameter and 14 mm in height chosen to minimize the dynamic effects. The sand part was made of 26000 particles with a polydispersity lying between ∅ 0.2 mm and ∅ 0.6 mm. The wire network was composed of 2900 beads of diameter ∅ 0.2 mm with a voluminal length density equal to 400 km.m^{-3}. The

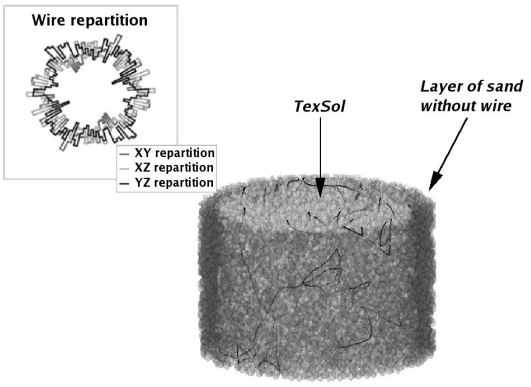

Fig. 8 *TexSol*$^{\text{TM}}$ sample before deposit on a rubber plan with the distribution of wire element directions projected on several plans ((O, x, y), (O, x, z) and (O, y, z)).

wire beads were connected with an *"elastic wire"* contact law. As shown in Fig. 8 the initial reinforcement network was quasi-equiprobably distributed. A periferic granular layer without any wires was added to the sample to compare the two domain behaviors. The particles was placed on a rubber plan by gravity until sample ki-

netic energy was close to zero; this part of the simulation took around 0.2 s. Our discrete simulation was made with 4000 time steps of 0.05 ms. Once the sample was stabilized, the wire network was seen to spread out (cf. Fig. 9). Indeed the reinforcement structure was mobile

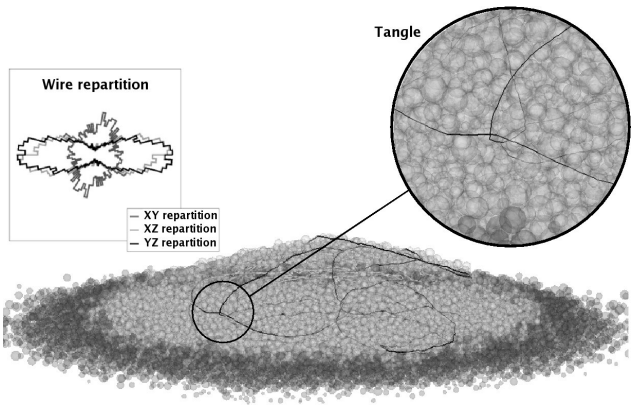

Fig. 9 *TexSol*$^{\mathrm{TM}}$ sample after deposit on a rubber plan with the distribution of wire element directions projected on several plans ((O,x,y), (O,x,z) and (O,y,z)).

and subsided following the sand particles. But this transformation leads the wire to form horizontal "stoppings" around the divergent particle flow which prevent sand circulation under gravity. The wire network becomes orthotropic with two main directions x and y as shown in Fig. 9. This large transformation implies that the wire crosses itself and consequently increases its tangles. The zoom represented in Fig. 9 illustrates that the two opposed movements of the two wire parts vanish; this creates a new wire anchoring point. The wire network was fixed by multiplying these anchoring points (resulting from tangles or blocking by sand). Reinforcement modify the final shape and contact force distribution. The averaged shapes, the averages pressures on the floor and their regressions are drawn in Fig. 10. A similar sample was made of 800 km.m^{-3} of wire. The shape regressions (linear for the sand, cubic for *TexSol*$^{\mathrm{TM}(1)}$, to the 8$^{\mathrm{th}}$ degree for *TexSol*$^{\mathrm{TM}(2)}$) were derived to find the maximum slope; the pressure regressions (cubic) smooth the phenomenon of contact concentration on hollow rings (due to the periodic distribution of the rubber plan beads). This graph confirms that the wire retains sand particles at the top of the sample. This effect increased with wire quantity. In both cases, the slope friction angle of the *TexSol*$^{\mathrm{TM}}$ θ_{t} was higher than the sand one θ_{s}; numerical and experimental values coincided [9] lying between 0° to 10°. Moreover, this simulation emphasized the paring arcs phenomenon of the granular assemblies described in [14]. Indeed, the floor pressure regressions show that they do not depend directly on the upside granular mass. In fact, granular slopes created chains of contact forces, like paring arcs, supporting the mass. The pressure plots

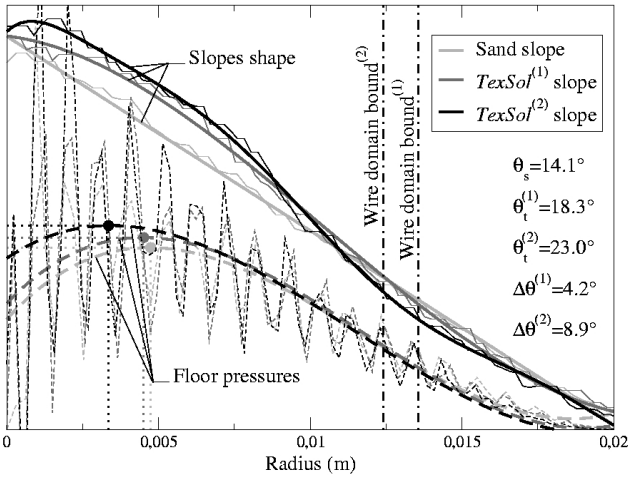

Fig. 10 Shape and pressure of sand, *TexSol*$^{\mathrm{TM}(1)}$ with a wire voluminal length density equal to 400 km.m^{-3} and *TexSol*$^{\mathrm{TM}(2)}$ with a wire voluminal length density equal to 800 km.m^{-3}.

maxima point out the effects of arc roots on the ground. The wire network increases these paring arc curvatures and intensity. In this test, reinforcement did not react directly, it simply increased the efficiency of existing granular mechanisms.

3.2 Wire network behavior on small strain tests

The previous section dealt with reinforcement mechanisms in large transformations. But with a small strain background the wire network is not as mobile and may not generate long distance interactions as previously. Therefore, a triaxial test was carried out on a box-shaped sample which is a three-dimensional extension of the biaxial one (cf. Sect. 2.3). The *TexSol*$^{\mathrm{TM}}$ sample of side 1.6 cm, included 8000 particles with 1500 to model a wire of voluminal length density 200 km.m^{-3}. This was subjected to a constant pressure around 15 kPa on the lateral sides and to a prescribed velocity of the upper side leading to a global deviatoric loading. The loading rate was chosen to avoid dynamic effect. The wire was modeled with an *"elastic wire"* contact law and the simulation was made with 100000 time steps of 0.05 ms. The wire was randomly distributed as shown in Fig. 11(a). The Force network between sand grains and wire beads is displayed in Fig. 11(b). The strong and weak networks, characteristic of granular assemblies can be distinguished [17], but a statistical study showed that the properties of force magnitude distribution were not significantly modified in comparision with standard granular media. Attention focused on the wire force network only (cf. Fig. 11(c)) which was in fully tensile state. To the naked eye, the wire seems to work mainly in the horizontal directions; this is more evident in the upper part. The following

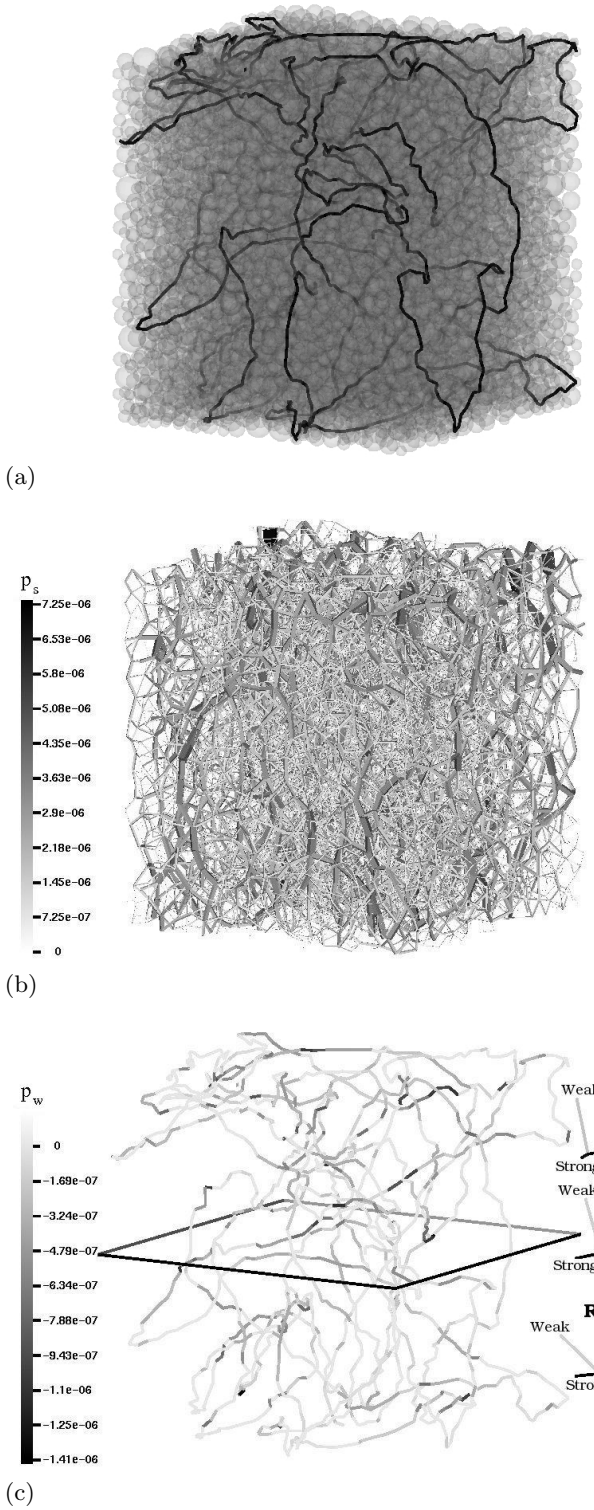

Fig. 11 Different views of a *TexSol*$^{\mathrm{TM}}$ box-shaped sample after a triaxial test: particles and wire position Fig. 11(a), contact forces network Fig. 11(b) and wire in tensile state Fig. 11(c). The last figure shows three frames R_u, R_l and R_g respectively the stress principal directions of the upper sample part, the lower sample part and the global sample. Precisions are added to these directions to distinguish the strong ones from the weak ones.

concepts attempt to quantify this feature. Considering a granular domain Ω of volume V_Ω including m particles and some contact forces, the Weber tensor [5] defines an average stress of Ω by

$$\boldsymbol{\sigma}_\Omega = \frac{1}{V_\Omega} \sum_{\alpha \in \Omega} l^\alpha \otimes p^\alpha \ , \tag{18}$$

where l^α is the inter-center vector of a contact α. To define a granular strain, the relative displacement of the p particle to an average displacement is introduced: $\widetilde{U}^p = U^p - \frac{1}{m}\sum_{p\in\Omega} U^p$. A similar formula defines the relative position: $\widetilde{X}^p = X^p - \frac{1}{m}\sum_{p\in\Omega} X^p$. In [3], Bagi analyze the formulation proposed by Cambou [4; 6] to be the best-fit for three-dimensional granular samples. This equivalent strain tensor $\boldsymbol{\varepsilon}_\Omega$ has to minimize the quadratic error of the equality $\widetilde{U}^p = \boldsymbol{\varepsilon}_\Omega \widetilde{X}^p$, leading to the expression

$$\boldsymbol{\varepsilon}_\Omega = \left(\sum_{e\in\Omega} \widetilde{X}^e \otimes \widetilde{X}^e \right)^{-1} : \left(\sum_{e\in\Omega} \widetilde{X}^e \otimes \widetilde{U}^e \right) \ . \tag{19}$$

The principal directions of the reinforcement stress tensor are drawn on the right side of Fig. 11(c). The principal stresses are all positive throughout the process; two of them (the horizontal ones) are dominant. The magnitude of the vertical principal direction is negligible; this means that the wire network does not work in the compressive direction. In fact, while compression occurs, particles move laterally, dragging the wire beads along; the wire is tensely solicited on the dilating horizontal plan. This phenomenon is clearly observable on the upper part ($\mathrm{R_u}$) because loading is applied on the upper side. On the lower part, particles are more static; the principal stresses are weak and their directions ($\mathrm{R_l}$) are chaotic throughout the loading path.

The parameters of the wire discrete model may have an influence on this mechanism, especially the diameter of the wire beads. To verify this, a little box-shaped *TexSol*$^{\mathrm{TM}}$ sample of 3700 particles was created; its wire was modeled by beads of diameter equal to that of the smallest sand particle. Two other samples were made with wires which respectively tripled and quadrupled the original number of beads at the same time dividing the original beads diameter by three and four as shown in Fig. 12. Despite few volumic differences, they are close enough in terms of wire and particle distribution (zooms of Fig. 12). The principal strains of the *TexSol*$^{\mathrm{TM}}$, the sand alone and the wire, are given with respect to time in Fig. 12 for three sizes of beads.

- $r_w = r_{\min}$, the principal strains are similar to the others throughout the process.
- $r_w = \frac{1}{3} r_{\min}$, the principal strains diverge from the outset of loading.
- $r_w = \frac{1}{4} r_{\min}$, the principal strains merge initially. Then they diverge from a critical instant; the gap increases in the horizontal directions.

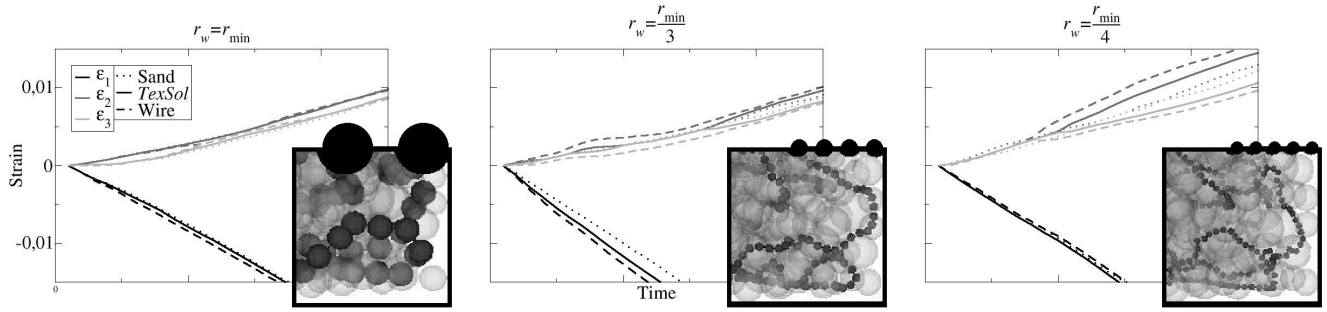

Fig. 12 Comparison of the equivalent strain tensor between several samples made with different wire size.

The related physical phenomenon is the sudden large sliding of the wire with respect to the sand. This sliding occurs in the same direction leading to a non symmetry of the two horizontal wire strains. The thinner the wire, the more it slips. These relative slidings conflict with the assumptions of the continuous model (cf. Sect. 1.2). Thus, if an identification approach is performed using discrete element investigations, the validity limits can be so defined.

3.3 Triaxial tests on cylinder-shaped samples

However, triaxial tests on box-shaped samples may introduce some edge effects (stress devolution). Cylinder-shaped samples were preferred to limit these parasite phenomena. The pressurization of such a sample was made by a specific procedure [18] which applies a confinement loading on free surface particles. A *TexSol*$^{\mathrm{TM}}$ granular medium was generated in a cylindrical container of 20 mm height and ∅ 9 mm, including 6200 sand particles lying between ∅ 0.3 mm and ∅ 0.8 mm, and 1100 wire beads with a lineic density equal to 250 km.m^{-3}. The deviatoric load was imposed by an upper-wall constant velocity and fixed bound conditions were simulated for the *TexSol*$^{\mathrm{TM}}$ sample to carry out a inhomogeneous mechanical test. Several "Unilateral" contact laws were compared in these simulations performed with 2000 time steps of 0.05 ms (without dynamic effects). The sample final state represented in Fig. 13(a) shapes like a barrel. This classic shape in continuum mechanics is obtained because sand particles try to spread out in the least constrained plan (maximum dilatancy plan) which, in our case, is the median horizontal one. The wire law used was the *"elastic wire"* with a lineic stiffness k equal to 1 N (force per strain). The initial unilateral behavior is recovered in Fig. 13(b). Consequently, wire spherical stress is a non negative value as the wire principal stresses. Using the Weber tensor (Eq. (18)), an equivalent wire stress map is given in Fig. 13(c) drawn in the axial/radial section. This proves that the wire works best in the maximum dilatancy plan in a tensile state. These results confirm the continuous modeling chosen in [10]. As mentioned in the previous section, a wire stress appears on the upper side of the sample and is due to asymmetric loading. Similar tests were carried out on several samples varying k, including a sand sample and a *TexSol*$^{\mathrm{TM}}$ made with a *"rigid wire"*. In Fig. 14 and 15, the behavior of

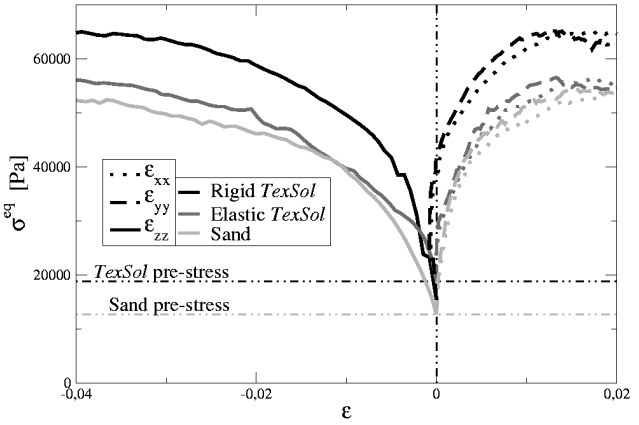

Fig. 14 Equivalent stress vs. strains plots for *TexSol*$^{\mathrm{TM}}$ and sand samples.

a "Rigid" *TexSol*$^{\mathrm{TM}}$ sample and an "Elastic" *TexSol*$^{\mathrm{TM}}$ sample of lineic stiffness $k = 0.2$ N is compared to a sand sample. On the stress vs. strain plots in Fig. 14, we can distinguish an initial quasi-elastic behavior. Then, some dissipative phenomena appear, due to micro-slips. For the same strain level at the end of the test, "Rigid" wire provides a 23% equivalent stress increase. Despite its great softness, "Elastic" wire improves mixture stiffness with a 7% stress increase. Sample preparation, especially the pressurization process, leads to initial stresses related to wire stiffness. The more the wire network is preloaded, the more it interacts with the sand grains; this explains the initial stress shift between sand and *TexSol*$^{\mathrm{TM}}$ underlined in Fig. 14.

During the process, the wire network stress level increased linearly as shown in Fig. 15. The reinforcement was considered as a linear elastic structure for both "Elastic" and "Rigid" contact laws, which is surprising for the rigid network. The first had a stress shift due to

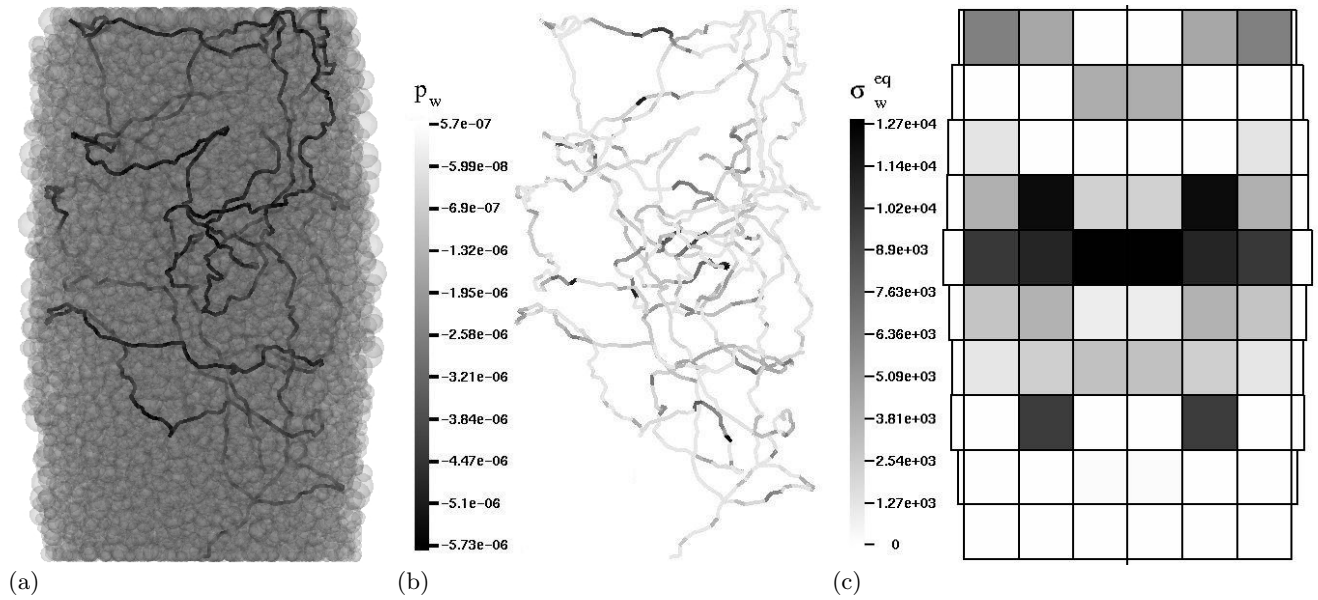

Fig. 13 Different views of a *TexSol*$^{\mathrm{TM}}$ cylinder-shaped sample after a triaxial test: particles and wire position in Fig. (a), wire in tensile state Fig. (b) and wire equivalent stress in Fig. (c) computed on several torus. The equivalent stress is defined as $\boldsymbol{\sigma}_w^{\mathrm{eq}} = ||\mathrm{dev}(\boldsymbol{\sigma}_w)||$.

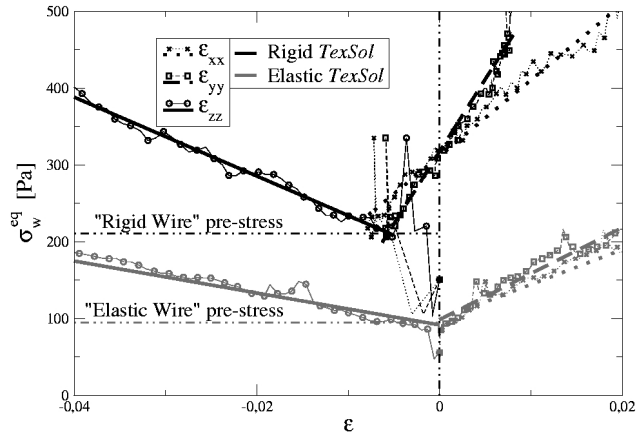

Fig. 15 Wire equivalent stress vs. strains plots for *TexSol*$^{\mathrm{TM}}$ samples.

Wire lineic stiffness k [N]	Wire equivalent stiffness H [N]	Linear starting point (ε%, [N])
0.1	1519	$(0, 90)$
0.2	3267	$(0, 90)$
0.5	3981	$(,)$
1	3563	$(0.2, 100)$
2	4303	$(,)$
5	4384	$(,)$
10	4479	$(0.3, 125)$
20	4603	$(,)$
50	3930	$(,)$
100	4695	$(,)$
∞	$H_\infty = 5142$	$(0.6, 230)$

Table 2 Wire network macro-stiffness vs. wire micro-stiffness.

the sample preparation above. This increased with wire stiffness but a strain shift appeared, especially for the "rigid wire". From the very start of the triaxial test, wire behavior was disturbed by a brutal contracting reorganization amplified for "rigid wire". To quantify the linear elastic behavior of the wire network, a representative macro-stiffness H was defined as the slope of a $(\varepsilon_{zz}, \sigma_w^{\mathrm{eq}})$ plot. Table 2 and Fig. 16 emphasize the non linear relation between micro-stiffness k and a macro one H. Moreover, it tended towards a limit represented by the macro-stiffness H_∞ of the "rigid wire" network.

4 Conclusion and perspectives

These numerical investigations using a discrete elements method highlight that different reinforcement mechanisms occur according to the strain level of the test. Non local phenomena like long distance interactions tend to appear in large transformations. The study also emphasizes the unilateral feature of the wire network. This experimental numerical study confirms two main points useful for further identification procedures. First, the strain rate equalities (cf. Sect. 1.2) are validated for a range of wire geometrical parameters (cf. Fig 12). Secondly, the unilateral feature of the wire network and its linear elastic behavior are underlined (cf. Fig 15). In this paper, we chose to illustrate the elastic macro-stiffness of the rein-

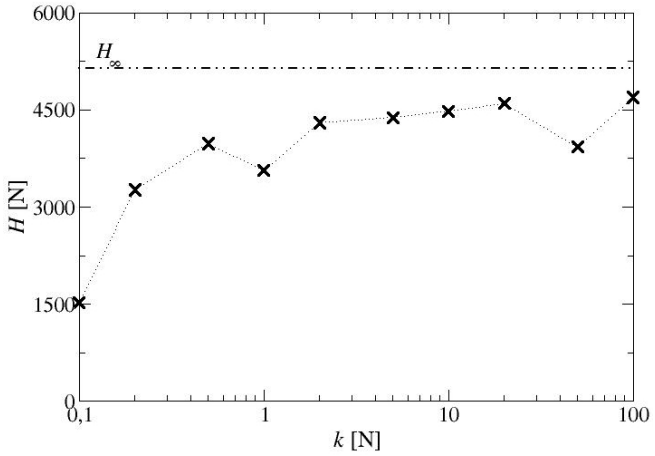

Fig. 16 Wire network macro-stiffness vs. wire micro-stiffness.

forcement using only one parameter. In the general case, the elastic tensor depends on micro-stiffness and wire lineic density, but may also depend on tangle, tortuosity et cætera.

References

1. S. Avril, M. Bonnet, A-S. Bretelle, M. Grédiac, F. Hild, P. Ienny, F. Latourte, D. Lemosse, S. Pagano, E. Pagnacco, and F. Pierron. Identification from measurements of mechanical fields. Draft, jun 2006.
2. K. Bagi. Stress and strain in granular assemblies. *Mechanics of materials*, (22):165–177, 1996.
3. K. Bagi. Microstructural strain tensors in granular assemblies. *International Journal of Solids and Structures*, (43):3166–3184, 2005.
4. B. Cambou, M. Chaze, and F. Dedecker. Change of scale in granular materials. *European Journal of Mechanics - A/Solids*, (19):999–1014, 2000.
5. B. Cambou and M. Jean. *Micromécanique des matériaux granulaires*. Hermès, Science-Paris, 2001.
6. F. Dedecker, M. Chaze, P. Dubujet, and B. Cambou. Specific features strain in granular materials. *Mech. Cohesive-Frictional Matter*, (5):173–193, 2000.
7. M. Fremond. *Non-Smooth Thermo-mechanics*. Springer-Verlag, Berlin Heidelberg New York, 2002.
8. M. Jean. The non smooth contact dynamics method. *Computer Methods in Applied Mechanic and Engineering*, (177 (Special issue)):235–257, 1999.
9. M. Khay and J-P. Gigan. Texsol - ouvrage de soutènement. Technical report, LCPC, 1990.
10. R. Laniel, P. Alart, and S. Pagano. Consistent thermodynamic modelling of wire-reinforced materials. *European Journal of Mechanics - A/Solids*, 2007. Accepted.
11. R. Laniel, O. Mouraille, S. Pagano, F. Dubois, and P. Alart. Numerical modelling of reinforced geomaterials by wires using the non smooth contact dynamics. In *Analysis and Simulation of Contact Problems*, pages 289–296, 2005.
12. E. Leflaive, M. Khay, and J-C. Blivet. Un nouveau matériaux: le texsol. *Travaux*, (602):1–3, 1985.
13. J. Lemaitre and J-L. Chaboche. *Mechanics of solid materials*. Cambridge, 1990.
14. J-J. Moreau. Numerical aspects of the sweeping process. *Comput. Methods Appl. Mech. Engrg.*, (177):329–349, 1999.
15. J-J. Moreau. Tenseur contrainte dans le granulats et autres collections d'objets. GDR MIDI, Carry-le-Rouet, jun 2005.
16. O. Mouraille. Etude sur le comportement d'un matériau à longueur interne: le texsol. Master's thesis, Université de Montpellier II, 2004.
17. F. Radjaï, D. E. Wolf, M. Jean, and J-J. Moreau. Bimodal character of stress transmission in granular packings. *Phys. Rev. Lett.*, 80(1):61–64, 1998.
18. A. Taboada, K-J. Chang, F. Radjaï, and F. Bouchette. Rheology, force transmission, and shear instabilities in frictional granular media from biaxial numerical tests using the contact dynamics method. *Journal of Geophysical Research*, 110:1–24, 2005.
19. P. Villard. *Etude du renforcement des sables par des fils continus*. PhD thesis, Université de Nantes, ENSM, 1988.